Temperature and pressure dependence of the addition reactions of HO to NO and to NO 2 . IV. Saturated laser-induced fluorescence measurements up to 1400 bar

D. Fulle, H. F. Hamann, H. Hippler, and J. Troe

Citation: The Journal of Chemical Physics **108**, 5391 (1998); doi: 10.1063/1.475971
View online: http://dx.doi.org/10.1063/1.475971
View Table of Contents: http://scitation.aip.org/content/aip/journal/jcp/108/13?ver=pdfcov
Published by the AIP Publishing

Temperature and pressure dependence of the addition reactions of HO to NO and to NO_2. IV. Saturated laser-induced fluorescence measurements up to 1400 bar

D. Fulle
Institut für Physikalische Chemie und Elektrochemie der Universität Karlsruhe, Kaiserstrasse 12, D-76128 Karlsruhe, Germany

H. F. Hamann
Institut für Physikalische Chemie der Universität Göttingen, Tammannstrasse 6, D-37077 Göttingen, Germany

H. Hippler
Institut für Physikalische Chemie und Electrochemie der Universität Karlsruhe, Kaiserstrasse 12, D-76128 Karlsruhe, Germany

J. Troe
Institut für Physikalische Chemie der Universität Göttingen, Tammannstrasse 6, D-37077 Göttingen, Germany

(Received 4 November 1997; accepted 24 December 1997)

The recombination reactions $HO+NO+M \Rightarrow HONO+M(1)$ and $HO+NO_2+M \Rightarrow HNO_3+M(2)$ have been investigated over an extended pressure (1–1000 bar) and temperature (250–400 K) range. HO radicals were generated by laser flash photolysis of suitable precursors and their decays were monitored by saturated laser-induced fluorescence (SLIF) under pseudo-first-order conditions. The measured rate constants were analyzed by constructing falloff curves which provide the high pressure limiting rate constants k_∞. In the given temperature range, these rate constants are $k_{1,\infty} = (3.3\pm 0.5)\times 10^{-11}\times (T/300\ \mathrm{K})^{-(0.3\pm 0.3)}$ and $k_{2,\infty} = (7.5\pm 2.2)\times 10^{-11}\ \mathrm{cm^3\ molecule^{-1}\ s^{-1}}$.
 [S0021-9606(98)01413-5]

I. INTRODUCTION

Rate constants of thermal dissociation and the reverse recombination reactions in the high pressure limit are directly related to the potential between the dissociation fragments. On the basis of the potential, the rate constants at higher temperatures can be established accurately by classical trajectory (CT) calculations or, under the conditions of adiabatic dynamics, equivalently by the statistical adiabatic channel model (SACM). The agreement (better than 0.2%) between CT and SACM in the classical range has been demonstrated recently for a series of model potentials such as ion–dipole, ion–quadrupole, dipole–dipole, and standard valence potentials.[1–4] Canonical variational transition state theory (CVTST) was shown[5] to perform much less satisfactorily.

Having in hand a reliable method to relate potential energy surfaces and high pressure recombination/dissociation rate constants, one is looking for suitable test systems where experiments and theory can be compared in a rigorous way. On the one hand, this requires measurements reading up to pressures where $k_{\mathrm{rec},\infty}$ can be obtained reliably by extrapolation. On the other hand, *ab initio* calculations of the potential energy surface have to be performed in a range of intermediate interparticle distances, which has been considered only in rare cases. It is of great importance to compare rate calculations based on such realistic potentials.[4] A first comparison of this type was given for the $NO+O \Leftrightarrow NO_2$ system.[6,7]

Continuing this search for suitable test reactions, in part I of this series[8] we followed the addition of HO radicals to HO, NO, and NO_2 up to the high pressure limit at 298 K. In part III,[9] measurements for the recombination $HO+HO \rightarrow H_2O_2$ were extended over a temperature range 200–400 K. In the present work, we measured the rate of the reaction,

$$HO+NO(+M) \rightarrow HONO(+M), \tag{1}$$

from 250 to 400 K; for the reaction

$$HO+NO_2(+M) \rightarrow HONO_2(+M), \tag{2}$$

temperatures between 268 and 400 K were applied while the pressure of the bath gas was increased up to 1400 bar. The wide pressure range of the present studies allowed the extrapolation of the falloff curves toward the high pressure limit with much better reliability than before. Likewise, the temperature coefficient of the high pressure limiting rate constant now could be established.

The present high pressure, recombination rate constants in a subsequent article[10] will be compared by SACM/CT calculations applied to *ab initio* potentials. The results then will also be compared with calculations using simpler dipole–dipole or standard valence potentials. We emphasize that fine details of the potential in reality do matter such that these treatments go far beyond the CVTST calculations with simplified potentials from Ref. 11 (for $HO+NO \Leftrightarrow HONO$).

Besides the described interest for testing unimolecular rate theory, reactions (1) and (2) are known to be important radical sinks in the atmosphere. Under low and medium pressure conditions, their rate coefficients have been measured extensively (see the recent evaluation in Ref. 12). The present work helps to establish a full set of falloff curves which extends to conditions which have not yet been realized in the laboratory. Furthermore, for reaction (2) there is a problem with the measurements between 0.1 and 1 bar which suggest a much lower high pressure limit of the rate coefficients than observed in Ref. 8. We investigated whether this problem persists also at temperatures other than 298 K. We also discuss whether this problem is an experimental artifact or whether one can imagine a ''kink'' in the falloff curve.

II. EXPERIMENTAL TECHNIQUE

The general experimental setup and the details of the saturated laser-induced fluorescence technique (SLIF), which in our work was used for HO detection, have been described before.[8,9,13] Only specific details of the experiments of the present work are mentioned in the following.

Three different methods for the generation of HO radicals by laser flash photolysis were used in our experiments. In measurements of reaction (2), nitric acid was photolyzed using an excimer laser at 248 nm (Lambda Physik EMG 200, KrF, 400 mJ, 20 ns) with a quantum yield of unity and an absorption cross section of $\sigma_3 = 2\times10^{-20}$ cm^2 molecule^{-1} at 298 K (Ref. 12) for

$$HNO_3 + h\nu \rightarrow HO + NO_2. \tag{3}$$

The high pressure mixture contained 1–2 mbar of HNO_3 and 0.5–2 mbar of NO_2. Therefore, the amount of NO_2 produced by photolysis as well as the reaction

$$HO + HNO_3 \rightarrow H_2O + NO_3 \tag{4}$$

[$k_4 = 1.5\times10^{-13}$ cm^3 molecule^{-1} s^{-1} (Ref. 12)] could be neglected.

For the investigation of reaction (1) at temperatures of 400 K we photolyzed N_2O at 193 nm (EMG 200, ArF, 200 mJ, 20 ns) with a quantum yield of unity and an absorption cross section of $\sigma_5 = 7.2\times10^{-20}$ cm^2 molecule^{-1} (Ref. 12) for

$$N_2O + h\nu \rightarrow N_2 + O(^1D). \tag{5}$$

The $O(^1D)$ atoms react fast with added H_2O through

$$O(^1D) + H_2O \rightarrow 2HO \tag{6}$$

[$k_6 = 2.2\times10^{-10}$ cm^3 molecule^{-1} s^{-1} (Ref. 12)]. The reactions

$$N_2O + O(^1D) \rightarrow 2NO, \tag{7}$$

$$N_2O + O(^1D) \rightarrow N_2 + O_2, \tag{8}$$

$$N_2O + O(^1D) \rightarrow N_2O + O(^3P), \tag{9}$$

$$NO + O(^1D) \rightarrow N + O_2 \tag{10}$$

[$k_7 = 7.2\times10^{-11}$, $k_8 = 4.4\times10^{-11}$, $k_9 < 10^{-12}$ (Ref. 12), $k_{10} = 8.5\times10^{-11}$ cm^3 molecule^{-1} s^{-1} (Ref. 14)] decrease the amount of the HO precursor $O(^1D)$. Our high pressure gas mixtures contained N_2O, H_2O, and NO with partial pressures of 40, 20, and 0.8–1.2 mbar, respectively. Under our conditions, 50% of $O(^1D)$ reacted to 2 HO, 15% reacted to 2 NO, and 35% reacted to $O(^3P)$. The amount of transient NO generated via reaction (4) was less than 1% of the NO initially present in the gas mixture.

The vapor pressure of H_2O decreases strongly at temperatures beyond 300 K. Therefore, as a radical precursor at 250 K we used 40 mbar of hydrogen instead of water, which gives HO through

$$O(^1D) + H_2 \rightarrow HO + H \tag{11}$$

[$k_{11} = 1.1\times10^{-10}$ cm^3 molecule^{-1} s^{-1} (Ref. 12)]. One can easily show that the hydrogen atoms produced in reaction (11) had no influence on the HO concentration time profiles. The reaction

$$HO + H_2 \rightarrow H_2O + H \tag{12}$$

[$k_{12} = 7.7\times10^{-12}\exp(-2100\ \mathrm{K}/T)$ cm^3 molecule^{-1} s^{-1} (Ref. 12)] also could be neglected at 250 K.

The high pressure mixtures were prepared in a 40 l stainless steel vessel for purified gases (Messer Griesheim) or in a homemade 8 l aluminum cylinder ($p < 50$ bar). In order to avoid accumulation of reaction products in the reaction cell, especially at low temperatures, the high pressure mixtures had to be exchanged continuously. At pressures below 8 bar, the high pressure mixture was flowing directly through the high pressure cell. The flow was controlled by needle valves (Hoke) and mass flow gauges (Tylan FC 260). Solenoid valves (Nova Swiss) at higher pressures were used to exchange the high pressure mixture in the cell after 15 laser shots (or more frequently). For the experiments at high pressures (200 bar and more), mixtures of HNO_3, NO_2, and helium or argon were introduced into the cell. These mixtures then were further pressurized with the bath gas using an oil-free diaphragm compressor (Nova Swiss). The total number of laser shots, which were taken to obtain one [HO]-time profile, was in this case reduced to an extent that the kinetics was not influenced by the accumulation of products or the loss of precursor molecules.

Two different types of high pressure cells were used. Experiments at pressures below 200 bar of helium (or argon) were performed with the ''low temperature cell'' described in Refs. 9 and 13. For experiments at pressures above 200 bar, we used the ''high temperature cell''.[9,13] The two windows (12×10 mm) for the pump and probe laser pulses, facing each other, as well as the detection window (8×10 mm) perpendicular to the laser axis were made from ultraviolet (UV) high quality sapphire (Steeg und Reuter). The cell was connected to a refill system containing high pressure valves (Nova Swiss) and stainless steel high pressure tubing (Nova Swiss, internal diameter 1.6, external diameter 6.35 mm).

The method of saturated laser-induced fluorescence (SLIF), such as described in Ref. 8, was used for the time-resolved detection of the HO radicals. An excimer laser (Lambda Physik EMG 201 MSC) operating at 308 nm (XeCl, 300 mJ, 20 ns) pumped a dye laser (Lambda Physik FL 3002 sulforhodamin B), which was frequency doubled

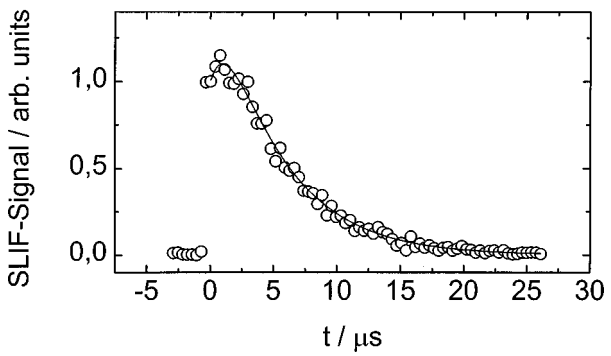

FIG. 1. SLIF time profile for reaction (1) at 250 K ($[He]=4.5\times10^{20}$ and $[NO]=8.5\times10^{15}$ molecule cm^{-3}). The solid line represents the best fit with $k_1=2.4\times10^{-11}$ cm^3 $molecule^{-1}$ s^{-1} in Eq. (15).

(BBO) and tuned to the $Q_1(2)$ line of the (0,0) vibrational band in the $A\,^2\Sigma^+\leftarrow X\,^2\Pi$ system of the HO radical at 307.995 nm.

N_2O, NO, NO_2, H_2, He, and Ar (Messer Griesheim, purities of >99.99%, 99.5%, 98%, 99.999%, 99.996%, 99.998%, respectively) were used without further purification. H_2O was demineralized and degassed. HNO_3 was distilled from a solution of 1:3 ppv of HNO_3 and H_2SO_4 (both supra pure grade) and collected at 77 K. The middle fraction was used after the purity had been checked by UV-absorption spectroscopy (Cary 5E).

III. EXPERIMENTAL RESULTS

A. Pressure and temperature dependence of the reaction HO+NO(+He)→HONO(+He)

Reaction (1) was investigated under pseudo-first-order conditions with an initial ratio $[HO]_0/[NO]_0$ of less than 2×10^{-2}. The falloff curve of the reaction was studied between 5 and 150 bar at 400 K and between 10 and 105 bar at 250 K. Our experiments near room temperature have been described previously.[8] At 400 K, monoexponential time profiles of the HO concentration were observed and expressed by the first-order rate law,

$$[HO]=[HO]_0\times\exp(-k_1[NO]t). \tag{13}$$

TABLE I. Second-order rate constants of reaction (1) HO +NO(+He)→HONO(+He) (No.=number of experiments).

T/K	p(He)/bar	[He]/(molecule cm^{-3})	k_1/(cm^3 molecule s^{-1})	No.
250	104	3.0×10^{21}	$(3.5\pm0.5)\times10^{-11}$	5
250	97	2.8×10^{21}	$(3.5\pm0.5)\times10^{-11}$	5
250	83	2.4×10^{21}	$(3.4\pm0.5)\times10^{-11}$	4
250	72	2.1×10^{21}	$(3.3\pm0.5)\times10^{-11}$	4
250	69	2.0×10^{21}	$(3.3\pm0.5)\times10^{-11}$	4
250	62	1.8×10^{21}	$(3.4\pm0.5)\times10^{-11}$	6
250	52	1.5×10^{21}	$(3.2\pm0.5)\times10^{-11}$	6
250	41	1.2×10^{21}	$(3.1\pm0.5)\times10^{-11}$	4
250	38	1.1×10^{21}	$(3.0\pm0.5)\times10^{-11}$	4
250	26.5	7.7×10^{20}	$(3.1\pm0.5)\times10^{-11}$	6
250	15.5	4.5×10^{20}	$(2.7\pm0.4)\times10^{-11}$	4
250	11	3.2×10^{20}	$(2.6\pm0.4)\times10^{-11}$	3
400	150	2.7×10^{21}	$(2.5\pm0.4)\times10^{-11}$	7
400	130	2.4×10^{21}	$(2.4\pm0.4)\times10^{-11}$	4
400	99	1.8×10^{21}	$(2.5\pm0.4)\times10^{-11}$	4
400	72	1.3×10^{21}	$(2.3\pm0.3)\times10^{-11}$	2
400	46	8.3×10^{20}	$(2.0\pm0.3)\times10^{-11}$	4
400	33	6.0×10^{20}	$(1.9\pm0.3)\times10^{-11}$	4
400	21.5	3.9×10^{20}	$(1.7\pm0.3)\times10^{-11}$	6
400	14	2.5×10^{20}	$(1.6\pm0.2)\times10^{-11}$	4
400	8.8	1.6×10^{20}	$(1.2\pm0.2)\times10^{-11}$	3
400	5.0	9.1×10^{19}	$(1.0\pm0.2)\times10^{-11}$	2

TABLE II. Second-order rate constants of reaction (2) HO $+NO_2$(+He)→HNO_3(+He) (*: nonideal gas; No.=number of experiments).

T/K	p(He)/bar	[He]/(molecule cm^{-3})	k_2/(cm^3 molecule $^{-1}$ s^{-1})	No.
268	140	3.8×10^{21}	$(6.5\pm1.0)\times10^{-11}$	8
268	122	3.3×10^{21}	$(6.4\pm1.0)\times10^{-11}$	6
268	104	2.8×10^{21}	$(6.3\pm1.0)\times10^{-11}$	8
268	85	2.3×10^{21}	$(6.1\pm1.0)\times10^{-11}$	8
268	63	1.7×10^{21}	$(6.0\pm1.0)\times10^{-11}$	8
268	44	1.2×10^{21}	$(5.2\pm0.8)\times10^{-11}$	13
268	29.5	8.0×10^{20}	$(4.8\pm0.7)\times10^{-11}$	6
268	20.5	5.5×10^{20}	$(4.6\pm0.7)\times10^{-11}$	4
268	15	4.0×10^{20}	$(4.2\pm0.6)\times10^{-11}$	7
268	9.2	2.5×10^{20}	$(4.0\pm0.6)\times10^{-11}$	7
268	5.5	1.5×10^{20}	$(3.9\pm0.6)\times10^{-11}$	4
268	3.7	1.0×10^{20}	$(2.9\pm0.4)\times10^{-11}$	3
268	2.8	7.6×10^{19}	$(2.5\pm0.4)\times10^{-11}$	1
268	1.7	4.6×10^{19}	$(2.2\pm0.3)\times10^{-11}$	4
268	1.2	3.3×10^{19}	$(1.96\pm0.3)\times10^{-11}$	4
268	1.04	2.8×10^{19}	$(1.4\pm0.2)\times10^{-11}$	2
300	1330	$*1.9\times10^{22}$	$(7.0\pm1.1)\times10^{-11}$	3
300	916	$*1.7\times10^{22}$	$(6.8\pm1.0)\times10^{-11}$	8
300	875	$*1.6\times10^{22}$	$(6.7\pm1.0)\times10^{-11}$	10
300	790	$*1.4\times10^{22}$	$(6.5\pm1.0)\times10^{-11}$	4
300	670	$*1.2\times10^{22}$	$(6.4\pm1.0)\times10^{-11}$	8
300	540	$*1.1\times10^{22}$	$(6.0\pm0.9)\times10^{-11}$	13
300	460	$*9.1\times10^{21}$	$(6.1\pm0.9)\times10^{-11}$	11
300	370	$*7.5\times10^{21}$	$(6.0\pm0.9)\times10^{-11}$	7
300	285	6.9×10^{21}	$(5.7\pm0.9)\times10^{-11}$	6
300	225	5.4×10^{21}	$(5.6\pm0.8)\times10^{-11}$	5
300	113	2.7×10^{21}	$(5.2\pm0.8)\times10^{-11}$	11
400	1370	$*1.7\times10^{22}$	$(6.2\pm0.9)\times10^{-11}$	2
400	890	$*1.2\times10^{22}$	$(5.8\pm0.9)\times10^{-11}$	9
400	775	$*1.1\times10^{22}$	$(5.6\pm0.8)\times10^{-11}$	4
400	610	$*9.4\times10^{21}$	$(4.9\pm0.7)\times10^{-11}$	6
400	515	$*8.1\times10^{21}$	$(5.1\pm0.8)\times10^{-11}$	4
400	425	$*6.8\times10^{21}$	$(4.7\pm0.7)\times10^{-11}$	6
400	320	5.8×10^{21}	$(4.4\pm0.7)\times10^{-11}$	7
400	230	4.2×10^{21}	$(3.9\pm0.6)\times10^{-11}$	8
400	177	3.2×10^{21}	$(3.8\pm0.6)\times10^{-11}$	3
400	150	2.7×10^{21}	$(3.5\pm0.5)\times10^{-11}$	8
400	127	2.3×10^{21}	$(3.3\pm0.5)\times10^{-11}$	14
400	105	1.9×10^{21}	$(3.5\pm0.5)\times10^{-11}$	6
400	99	1.8×10^{21}	$(3.2\pm0.5)\times10^{-11}$	8
400	72	1.3×10^{21}	$(3.0\pm0.4)\times10^{-11}$	5
400	44	7.9×10^{20}	$(2.6\pm0.4)\times10^{-11}$	8
400	34	6.1×10^{20}	$(2.2\pm0.3)\times10^{-11}$	14
400	21	3.8×10^{20}	$(2.0\pm0.3)\times10^{-11}$	10
400	14	2.5×10^{20}	$(1.6\pm0.2)\times10^{-11}$	2
400	8.8	1.6×10^{20}	$(1.4\pm0.2)\times10^{-11}$	4
400	5.0	9.1×10^{19}	$(1.1\pm0.2)\times10^{-11}$	3
400	3.0	5.4×10^{19}	$(1.2\pm0.2)\times10^{-11}$	4
400	2.5	4.5×10^{19}	$(0.8\pm0.2)\times10^{-11}$	2
400	1.9	3.5×10^{19}	$(0.7\pm0.1)\times10^{-11}$	1
400	1.6	2.9×10^{19}	$(0.6\pm0.1)\times10^{-11}$	4

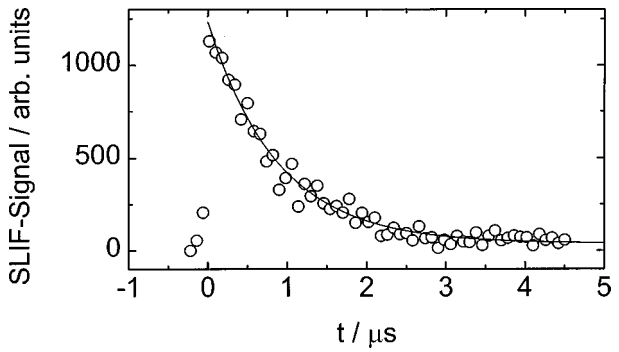

FIG. 2. SLIF time profile for reaction (2) at 400 K ([He]$=1.2\times10^{22}$ and [NO_2]$=2.1\times10^{16}$ molecule cm^{-3}). The solid line represents the best fit with $k_1=5.5\times10^{-11}$ cm^3 molecule^{-1} s^{-1} in Eq. (22).

In the absence of H_2O in the high pressure mixture at 250 K, the relaxation of vibrationally excited HO, formed by reaction (11) was so slow[15] that an increase of the population of HO($v=0$) was observed during the first μs, see Fig. 1. HO($v=0$) is formed by collisional quenching

$$\mathrm{HO}(v\geqslant1)(+X)\rightarrow\mathrm{HO}(v=0)(+X). \tag{14}$$

The SLIF profiles could well be represented by

$$[\mathrm{HO}(\nu=0)]=A\exp(-k_{14}t)+([\mathrm{HO}(\nu=0)]_0-A)\times\exp(-k_1[\mathrm{NO}]t) \tag{15}$$

with

$$A=\frac{k_{14}[\mathrm{HO}(\nu\geqslant1)]}{k_1[\mathrm{NO}]-k_{14}}. \tag{16}$$

k_{14} represents an effective pseudo-first-order quenching rate constant which depends on the individual quenching rate constants of the molecules in the high pressure mixture and their concentrations. Our measurements were not extended to temperatures below 250 K, because the photolysis of N_2O here becomes too inefficient due to the temperature dependence of the absorption cross section [$\sigma_5=5.2\times10^{-19}\times\exp(-590\ \mathrm{K}/T)$ cm^2 molecule^{-1} (Refs. 12 and 16) between 250 and 1200 K). Our results of the pseudo-second-order rate constants k_1 are given summarized in Table I.

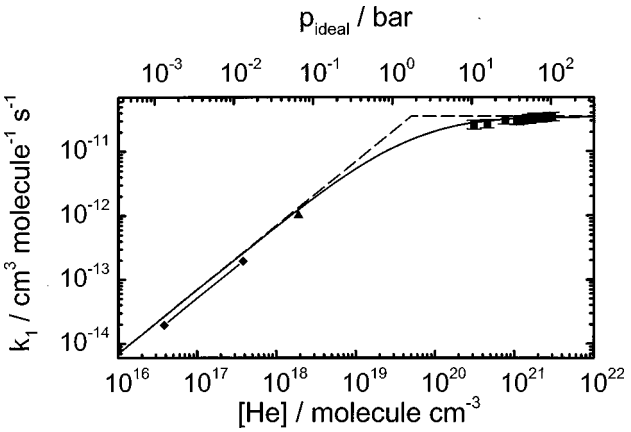

FIG. 3. Second-order rate constant k_1 for the reaction HO+NO (+M)⇒HONO(+M) at $T=250$ K with M=He (■: this work; ◆: interpolated from Ref. 21; ▲: Ref. 23; the solid line represents the best fit with Eqs. (17) and (18) using $k_{1,0}=7.0\times10^{-31}$ [He] cm^6 molecule^{-2} s^{-1}, $F_{1,\mathrm{cent}}=0.86$, and $k_{1,\infty}=3.5\times10^{-11}$ cm^3 molecule^{-1} s^{-1}).

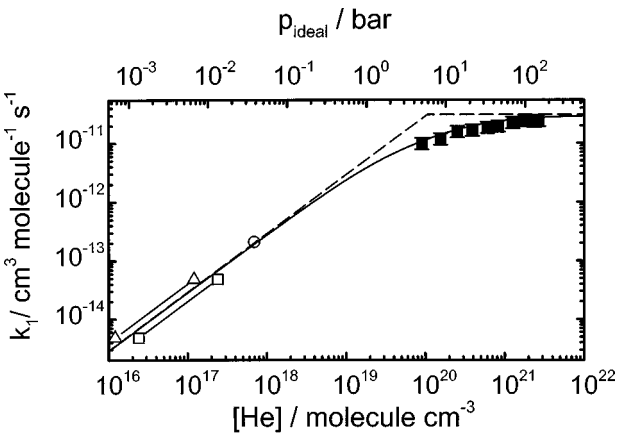

FIG. 4. Second-order rate constant k_1 for the reaction HO +NO(+M)⇒HONO(+M) at $T=400$ K with M=He (■: this work; ○: Ref. 20; □: Ref. 21; △: Ref. 22; the solid line represents the best fit with Eqs. (17) and (18) using $k_{1,0}=2.9\times10^{-31}$ [He] cm^6 molecule^{-2} s^{-1}, $F_{1,\mathrm{cent}}=0.75$, and $k_{1,\infty}=3.1\times10^{-11}$ cm^3 molecule^{-1} s^{-1}).

We represent the pressure dependence of k_1 using the formalism described in Refs. 17–19, i.e., writing

$$k_1=\left[\frac{k_{1,0}}{1+k_{1,0}/k_{1,\infty}}\right]\times F_{1,\mathrm{cent}}^{(1+(\log(k_{1,0}/k_{1,\infty})/N)^2)^{-1}}, \tag{17}$$

with

$$N=0.75-1.27\log(F_{1,\mathrm{cent}}). \tag{18}$$

Following Refs. 8, 12, and 20–23, the experimental low pressure rate constants $k_{1,0}$ for M=He are given by

$$k_{1,0}=6.0\times10^{-31}(T/300\ \mathrm{K})^{-2.5}[\mathrm{He}]\ \mathrm{cm^6\ molecule^{-2}\ s^{-1}}. \tag{19}$$

Broadening factors $F_{1,\mathrm{cent}}$ were theoretically estimated to be 0.86, 0.81, and 0.75 at 250, 300, and 400 K, respectively,[12] (see also the recent measurements in Refs. 24 and 25). Using Eqs. (17) and (18), the low pressure rate constant in Eq. (19), and the calculated $F_{1,\mathrm{cent}}$, the experiments were fitted and $k_{1,\infty}$ was derived. Figures 3 and 4 show the corresponding

TABLE III. Second-order rate constants of reaction (2) HO +NO_2(+Ar)→HNO_3(+Ar) (*: nonideal gas; No.=number of experiments).

T/K	P(Ar)/bar	[Ar]/(molecule cm^{-3})	k_2/(cm^3 molecule^{-1} s^{-1})	No.
300	97	2.3×10^{21}	$(6.0\pm1.5)\times10^{-11}$	11
300	5.8	1.4×10^{20}	$(2.4\pm0.4)\times10^{-11}$	7
300	3.8	9.3×10^{19}	$(2.2\pm0.3)\times10^{-11}$	4
300	2.3	5.4×10^{19}	$(1.7\pm0.3)\times10^{-11}$	4
400	400	$*6.4\times10^{21}$	$(4.7\pm1.2)\times10^{-11}$	2
400	320	$*5.4\times10^{21}$	$(5.6\pm1.4)\times10^{-11}$	4
400	245	4.4×10^{21}	$(4.4\pm1.1)\times10^{-11}$	4
400	200	3.6×10^{21}	$(3.3\pm0.8)\times10^{-11}$	3
400	155	2.8×10^{21}	$(3.8\pm1.0)\times10^{-11}$	2
400	95	1.7×10^{21}	$(3.5\pm0.9)\times10^{-11}$	4
400	90	1.6×10^{21}	$(2.9\pm0.7)\times10^{-11}$	3

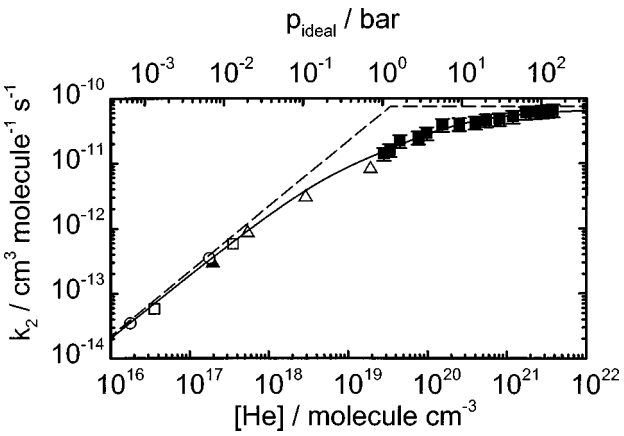

FIG. 5. Second-order rate constant k_2 for the reaction HO $+NO_2(+M) \Rightarrow HNO_3(+M)$ at $T=268$ K with M=He (■: this work; ○: Ref. 20 ($T=273$ K); □: interpolated from Ref. 21; △: Ref. 39 ($T=247$ K); ▲: Ref. 41 ($T=263$ K); the solid line represents the best fit with Eqs. (17) and (18) using $k_{2,0}=2.2\times10^{-30}$ [He] cm^6 molecule^{-2} s^{-1}, $F_{2,\mathrm{cent}}=0.45$, and $k_{2,\infty}=7.5\times10^{-11}$ cm^3 molecule^{-1} s^{-1}).

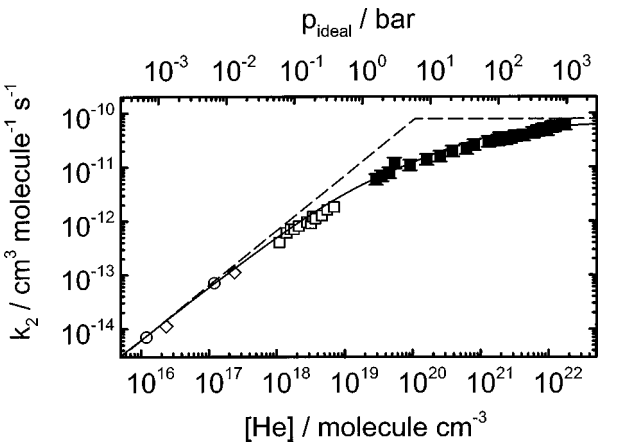

FIG. 7. Second-order rate constant k_2 for the reaction HO $+NO_2(+M) \Rightarrow HNO_3(+M)$ at $T=400$ K with M=He (■: this work, ○: Ref. 20 ($T=395$ K); ◇: interpolated from Ref. 21; □: Ref. 22 ($T=416$ K); the solid line represents the best fit with Eqs. (17) and (18) using $k_{2,0}=6.9\times10^{-30}$ [He] cm^6 molecule^{-2} s^{-1}, $F_{2,\mathrm{cent}}=0.33$, and $k_{2,\infty}=7.5\times10^{-11}$ cm^{-3} molecule^{-1} s^{-1}).

falloff curves for 250 and 400 K together with the data from Refs. 20–23. The derived limiting high pressure rate constants are

$$k_{1,\infty}=3.5\times10^{-11}\ \mathrm{cm^3\,molecule^{-1}\,s^{-1}}\ \text{at 250 K}$$
$$=3.3\times10^{-11}\ \mathrm{cm^3\,molecule^{-1}\,s^{-1}}\ \text{at 298 K}$$
$$=3.1\times10^{-11}\ \mathrm{cm^3\,molecule^{-1}\,s^{-1}}\ \text{at 400 K}, \quad (20)$$

which leads to

$$k_{1,\infty}=(3.3\pm0.5)\times10^{-11}(T/300\ \mathrm{K})^{-(0.3\pm0.3)}\ \mathrm{cm^3\,molecule^{-1}\,s^{-1}}. \quad (21)$$

The change of $k_{1,\infty}$ with temperature is too small to be established with certainty.

B. Pressure and temperature dependence of the reaction $HO+NO_2(+M)\rightarrow HONO_2(+M)$

Reaction (2) was investigated under pseudo-first-order conditions with an initial ratio of $[HO]_0/[NO_2]_0$ less than 10^{-2}. With the bath gas helium, temperatures between 268 and 400 K and pressures up to 1400 bar were employed; experiments with the bath gas argon were performed at 300 and 400 K, and at pressures up to 400 bar. Under all conditions, HO radicals were produced by photolysis of HNO_3 such as described in the previous section. Monoexponential HO profiles were observed, see Fig. 2, and evaluated by

$$[HO]=[HO]_0\exp(-k_2[NO_2]t). \quad (22)$$

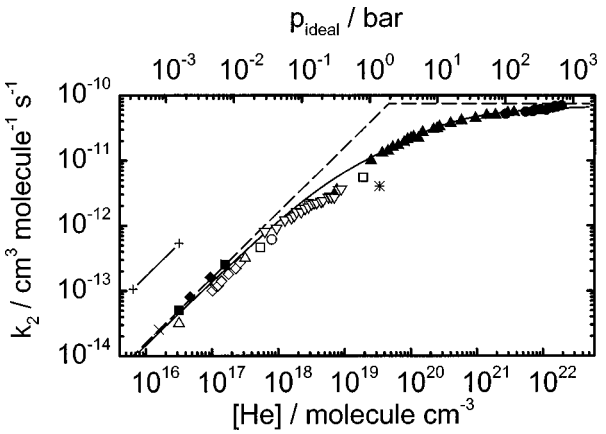

FIG. 6. Second-order rate constant k_2 for the reaction HO $+NO_2(+M) \Rightarrow HNO_3(+M)$ at $T=300$ K with M=He (●: this work; ▲: Ref. 8; □: Ref. 39; ◇: Ref. 41; ×: Ref. 20; △: Ref. 21; ▽: Ref. 22; ○: Ref. 40, ■: Ref. 34; +: Ref. 37; ♦: Ref. 36; *: Ref. 35; the solid line represents the best fit with Eqs. (17) and (18) using $k_{2,0}=1.6\times10^{-30}$[He] cm^6 molecule^{-2} s^{-1}, $F_{2,\mathrm{cent}}=0.41$, and $k_{2,\infty}=7.5\times10^{-11}$ cm^3 molecule^{-1} s^{-1}).

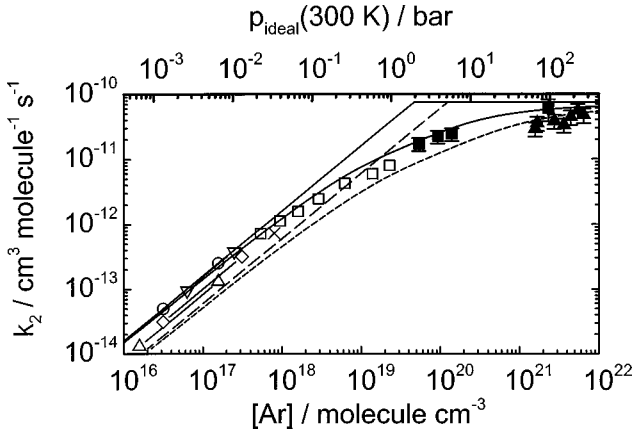

FIG. 8. Second-order rate constant k_2 for the reaction HO $+NO_2(+M) \Rightarrow HNO_3(+M)$ at $T=300$ K (400 K) with M=Ar (■: this work (300 K); ▲: this work (400 K); □: Ref. 39; △: Ref. 20; ◇: Ref. 22; ×: Ref. 40; ○: Ref. 34; ▽: Ref. 38; the solid line represents the best fit for 300 K with Eqs. (17) and (18) using $k_{2,0}=1.6\times10^{-30}$ [Ar] cm^6 molecule^{-2} s^{-1}, $F_{2,\mathrm{cent}}=0.47$, and $k_{2,\infty}=7.5\times10^{-11}$ cm^3 molecule^{-1} s^{-1}; the dashed line represents the best fit for 400 K with Eqs. (17) and (18) using $k_{2,0}=6.0\times10^{-30}$ [Ar] cm^6 molecule^{-2} s^{-1}, $F_{2,\mathrm{cent}}=0.37$, and $k_{2,\infty}=7.5\times10^{-11}$ cm^3 molecule^{-1} s^{-1}).

TABLE IV. Summary of rate constant parameters for reaction (1) HO+NO(+M)→HONO(+M).

	M=He	M=He	M=He
T/K	268	300	400
k_∞ / cm^3 molecule^{-1} s^{-1}	3.5×10^{-11}	3.3×10^{-11}	3.1×10^{-11}
k_0/[M] / cm^6 molecule^{-2} s^{-1}	6.0×10^{-31}	4.0×10^{-31}	2.0×10^{-31}
β_c	0.13	0.11	0.09
$-\langle\overline{\Delta E}\rangle$/cm^{-1}	38	34	36
F_{cent}	0.90	0.86	0.75

The experimental values of k_2 are given in Table II for M=He and in Table III for M=Ar. Below 300 bar, the total gas density $[M]$ was calculated by the perfect gas law. At higher pressures, real gas effects were taken into account.[26,27]

The falloff curve of reaction (2) at 300 K was discussed in Ref. 8. The falloff curve seems to be broader than that for reaction (1) such that the extrapolation to the high pressure limit remained somewhat uncertain. Therefore, an extension to even higher densities than employed in Ref. 8 appeared desirable for a reliable extrapolation. Also an 'irregularity' in the falloff curve between 0.1 and 1 bar had to be reinspected. In order to investigate the bath gas dependence of the falloff curve, measurements with argon were also performed. It is well established that argon forms van der Waals complexes with HO radicals.[28–31] This might influence the pressure dependence of the falloff curve, if the energy transfer mechanism is overrun by the radical-complex mechanism, such as found for the recombination reaction Cl+O$_2$→ClOO.[32] Control of the reaction by diffusion can be neglected under our experimental conditions.[33]

The previous experiments led to a limiting low pressure rate constant $k_{2,0}$ of Refs. 8, 12 and 34

$$k_{2,0}=1.6\times10^{-30}(T/300\ \text{K})^{-2.9}[\text{He}]\ \text{cm}^6\,\text{molecule}^{-2}\,\text{s}^{-1}, \tag{23}$$

$$k_{2,0}=1.6\times10^{-30}[\text{Ar}]\ \text{cm}^6\,\text{molecule}^{-2}\,\text{s}^{-1}\ \text{at}\ 300\ \text{K}. \tag{24}$$

The temperature dependence of $k_{2,0}$ for M=Ar has not been investigated experimentally but it should be similar to that of helium. Broadening factors $F_{2,\text{cent}}$ were derived from theory to be 0.45 (268 K), 0.41 (300 K), and 0.33 (400 K).[12] Choosing a temperature independent high pressure limiting rate constant of 7.5×10^{-11} cm^3 molecules^{-1} s^{-1}, the experimental data are well reproduced by Eqs. (17), (18), (22), and (23), and the calculated $F_{2,\text{cent}}$. Together with low pressure data from the literature,[8,20–22,34–41] our data for M=He are plotted in Figs. 5, 6, and 7 at 268, 300, and 400 K, respectively. The high pressure measurements from this work confirm the earlier extrapolation to the high pressure limit.[8] The experiments at 400 and 268 K indicate that the high pressure limiting rate constant within an accuracy of ±20% is indeed temperature independent. Because of the lack of low pressure experiments at 400 K, the data obtained in argon at 300 and 400 K are plotted together in one falloff representation (see Fig. 8). More efficient quenching of HO ($^2\Sigma$) by argon reduces the fluorescence signal at higher pressures. The errors of the experimental rate constants are estimated to be 25% at pressures higher than 80 bar. Nevertheless, the results are in good agreement with the helium falloff data. Again, the high pressure limiting rate constant is extrapolated to be $k_{2,\infty}=7.5\times10^{-11}$ cm^3 molecule^{-1} s^{-1} (uncertainty of 30%). The values of the experimental rate constants at 400 are slightly lower than for 300 K, because the limiting low pressure rate constant has a negative temperature coefficient.

The new experiments have not brought an unambiguous answer to the question of whether the ''irregularity'' of the falloff curve of reaction with M=He between 0.1 and 1 bar (see Fig. 6) is real or an artifact. It seems that the ''effect'' is much less pronounced at 268 and 400 than at 300 K; also it is smaller for M=Ar. Before attributing this to experimental errors, however, one should keep in mind that quite anomalous ''falloff'' curves were observed in the recombination O+O$_2$(+M)→O$_3$(+M)[42] which changed their appearance over comparably small temperature intervals. Besides the competition of energy-transfer and radical-complex mechanisms (and other effects) probably responsible for the O$_3$ anomalies, in the HNO$_3$ system one may also still think of complications due to ''isomer'' formations, although their contribution at other occasions has been ruled out.[12]

IV. CONCLUSIONS

The results described in Sec. III provide limiting low and high pressure rate constants as well as broadening factors of the falloff curves which, together with Eqs. (17) and (18), reproduce experimental rate constants over wide ranges of temperature. The relevant values are summarized in Tables IV and V. We have to emphasize that we have not been able

TABLE V. Summary of rate constant parameters for reaction (2) HO+NO$_2$(+M)→HNO$_3$(+M).

	M=He	M=He	M=He	M=Ar	M=Ar
T/K	268	300	400	300	400
k_∞ / cm^3 molecule^{-1} s^{-1}	7.6×10^{-11}	7.5×10^{-11}	7.8×10^{-11}	7.5×10^{-11}	7.5×10^{-11}
k_0/[M] / cm^6 molecule^{-2} s^{-1}	2.2×10^{-30}	1.6×10^{-30}	6.9×10^{-31}	1.6×10^{-30}	6.0×10^{-31}
β_c	0.13	0.12	0.09	0.19	0.15
$-\langle\overline{\Delta E}\rangle$/cm^{-1}	40	41	39	75	75
F_{cent}	0.45	0.41	0.33	0.47	0.37

to prove or to disprove the mentioned irregularity of the rate coefficient k_2 between 0.1 and 1 bar at temperatures near 300 K. The data in Table V ''override'' this problem (see Fig. 6).

Tables IV and V are recommended for modeling the pressure dependence of reactions (1) and (2), see also Ref. 12. We leave the theoretical analysis of $k_{1,\infty}$ and $k_{2,\infty}$, such as described in the Introduction, to a later publication.[10] At this stage we only comment on the weak (if not negligible) temperature dependence of $k_{\mathrm{rec},\infty}$. Part of the temperature dependence may come from electronic partition functions of HO ($^2\Pi_{3/2}$ and $^2\Pi_{1/2}$) and NO ($^2\Pi_{1/2}$ and $^2\Pi_{3/2}$). Under the assumption that only the lowest fine structure components of HO, i.e., $^2\Pi_{3/2}$, and of NO, i.e., $^2\Pi_{1/2}$, lead to complex formation, the high pressure rate constant $k_{\mathrm{rec},\infty}$ contains the product of the inverse electronic partition functions of the recombining radicals. The energy splitting of 139.7 cm^{-1} between the fine structure components for HO[43] and of 121.1 cm^{-1} for NO,[43] respectively, determines the temperature dependence of the electronic partition function. Within the temperature range between 250 and 400 K, a temperature coefficient of $T^{-0.44}$ is obtained for $[Q_{el}(\mathrm{HO}) \times Q_{el}(\mathrm{NO})]^{-1}$ compared to the somewhat lower temperature coefficient of $T^{-0.3}$ for $k_{1,\infty}$. For reaction (2), the situation is very similar and the temperature coefficient of $T^{-0.21}$ for $[Q_{el}(\mathrm{OH}) \times Q_{el}(\mathrm{NO})_2]^{-1}$ may be hidden behind the temperature independent rate constant $k_{2,\infty}$. Before deciding whether there is this contribution,[7,44] *ab initio* calculations of excited state potentials have to be available, which show whether excited HO and/or NO without barriers lead to excited HONO or HNO_3. Independent of the corresponding possible weak temperature dependence, our measurements do not show signs of any marked temperature dependence of $k_{\mathrm{rec},\infty}$ in contrast to that of $k_{\mathrm{rec},0}$. This is in agreement with the corresponding observations of the O+NO system treated in detail before.[7] A more detailed analysis of this feature awaits the treatment in Ref. 10.

ACKNOWLEDGMENTS

Financial support of this work by the Deutsche Forschungsgemeinschaft (SFB 357 ''Molekulare Mechanismen unimolekularer Prozesse'') is gratefully acknowledged.

[1] J. Troe, J. Chem. Phys. **87**, 2773 (1987); **105**, 6249 (1996); A. I. Maergoiz, E. E. Nikitin, J. Troe, and V. G. Ushakov, *ibid.* , 6263 (1996).
[2] S. C. Smith and J. Troe, J. Chem. Phys. **97**, 5451 (1992); A. I. Maergoiz, E. E. Nikitin, J. Troe, and V. G. Ushakov, *ibid.* **105**, 6270 (1996).
[3] A. I. Maergoiz, E. E. Nikitin, J. Troe, and V. G. Ushakov, J. Chem. Phys. **105**, 6277 (1998).
[4] A. I. Maergoiz, E. E. Nikitin, J. Troe, and V. G. Ushakov, J. Chem. Phys. (to be published).
[5] J. Troe, Adv. Chem. Phys. **101**, 819 (1997).
[6] H. Hippler, M. Siefke, H. Stark, and J. Troe J. Chem. Phys. (to be published).
[7] L. B. Harding, H. Stark, and J. Troe, J. Chem. Phys. (to be published).
[8] R. Forster, M. Frost, D. Fulle, H. F. Hamann, H. Hippler, A. Schlepegrell, and J. Troe, J. Chem. Phys. **103**, 2949 (1995).
[9] D. Fulle, H. F. Hamann, H. Hippler, and J. Troe, J. Chem. Phys. **105**, 1001 (1996).
[10] L. B. Harding and J. Troe (to be published).
[11] M. T. Nguyen, R. Sumathi, D. Sengupta, and J. Peeters, Chem. Phys. (in press).
[12] R. Atkinson, D. L. Baulch, R. A. Cox, R. F. Hampson, J. A. Kerr, and J. Troe, J. Phys. Chem. Ref. Data **21**, 411 (1992); *ibid.* **26**, 521 (1997).
[13] D. Fulle, H. F. Hamann, H. Hippler, and J. Troe, J. Chem. Phys. **105**, 983 (1996).
[14] R. F. Heidner III, and D. Husain, Int. J. Chem. Kinet. **5**, 819 (1973).
[15] G. P. Glass, H. Endo, and B. K. Chaturvedi, J. Chem. Phys. **77**, 5450 (1982).
[16] M. G. Holliday and B. G. Reuben, Trans. Faraday Soc. **64**, 1735 (1968).
[17] J. Troe, J. Phys. Chem. **83**, 114 (1979).
[18] J. Troe, Ber. Bunsenges. Phys. Chem. **87**, 161 (1983).
[19] R. G. Gilbert, K. Luther, and J. Troe, Ber. Bunsenges. Phys. Chem. **87**, 169 (1983).
[20] A. A. Westenberg and N. de Haas, J. Chem. Phys. **57**, 5357 (1972).
[21] J. G. Anderson, J. J. Margitan, and F. Kaufman, J. Chem. Phys. **60**, 3310 (1975).
[22] C. Morley and I. W. M. Smith, J. Chem. Soc. Faraday Trans. II **68**, 1016 (1971).
[23] E. R. Lovejoy, T. P. Murrells, A. R. Ravishankara, and C. J. Howard, J. Phys. Chem. **94**, 2386 (1990).
[24] P. Pagsberg, E. Bjegbakke, E. Ratajczak, and A. Sillesen, Chem. Phys. Lett. **272**, 386 (1997).
[25] D. B. Atkinson and M. A. Smith, J. Phys. Chem. **98**, 5797 (1994).
[26] *Gas Encyclopedia, L'Air Liquide* (Elsevier Science, Amsterdam, 1976).
[27] S. Angus, K. M. Reuck, and R. D. McCarty, *International Thermodynamic Tables of the Fluid State, IUPAC* (Pergamon, New York, 1977).
[28] M. I. Lester, M. T. Berry, M. R. Brustein, C. Chakravarty, and D. C. Clary, Chem. Phys. Lett. **178**, 301 (1991).
[29] A. D. Esposti and H. J. Werner, J. Chem. Phys. **93**, 3351 (1990).
[30] C. Chakravarty and D. C. Clary, J. Chem. Phys. **94**, 4149 (1991).
[31] A. D. Esposti, A. Berning, and H.-J. Werner, J. Chem. Phys. **103**, 2067 (1995).
[32] S. Bear, H. Hippler, R. Rahn, M. Siefke, N. Seitzinger, and J. Troe, J. Chem. Phys. **95**, 6463 (1991).
[33] J. Troe, J. Phys. Chem. **90**, 357 (1986).
[34] J. P. Burrows, T. J. Wallington, and R. P. Wayne, J. Chem. Soc. Faraday Trans. II **79**, 111 (1983).
[35] E. Simonaitis and J. Heiklen, Int. J. Chem. Kinet. **4**, 529 (1972).
[36] L. G. Anderson, J. Phys. Chem. **84**, 2152 (1980).
[37] M. F. R. Mulcahy and R. H. Smith, J. Chem. Phys. **54**, 5215 (1971).
[38] G. W. Harris and R. P. Wayne, J. Chem. Soc. Faraday Trans. II **71**, 610 (1975).
[39] P. H. Wine, N. M. Kreutter, and A. R. Ravishankara, J. Phys. Chem. **83**, 3191 (1979).
[40] C. Anastasi and I. W. M. Smith, J. Chem. Soc. Faraday Trans. II **72**, 1459 (1976).
[41] K. Erler, D. Field, R. Zellner, and I. W. M. Smith, Ber. Bunsenges. Phys. Chem. **81**, 22 (1977).
[42] H. Hippler, R. Rahn, and J. Troe, J. Chem. Phys. **93**, 6560 (1990).
[43] M. W. Chase, Jr., C. A. Davies, J. R. Downey, Jr., D. J. Frurip, R. A. McDonald, and A. N. Syverud, J. Phys. Chem. Ref. Data Suppl. **14**, 1 (1985).
[44] I. W. M. Smith, Int. J. Chem. Kinet. **16**, 423 (1984).